First Airborne Trial of a UAV Based Optical Locust Tracker

Graham Brooker, Jeremy Randle, Muhammad Esa Attia, Zhe Xu, Tariq Abuhashim, Abdallah Kassir, Jen Jen Chung, Salah Sukkarieh, Nazifa Tahir
Australian Centre for Field Robotics,
Rose St Building (J04), University of Sydney, NSW 2006.
gbrooker@acfr.usyd.edu.au
John Dickens
CSIR Centre for Mining Innovation
PO Box 91230, Auckland Park 2006, Johannesburg, South Africa.

Abstract

A novel sensor has been developed to track the movement of individual Australian plague locusts from a UAV. It consists of a powerful strobe collocated with a camera which is able to detect returns from small (2.5mm) glass retro-reflectors mounted on the locusts, at ranges in excess of 100m. The paper discusses the development of an annular strobe surrounding a camera which maximises the amount of light returned to the camera. Hardware and software developed for the sensor are outlined along with problems with, and solutions to, strobe generated EMI effects on other aircraft electronics. Positive results of the ground tests and those from a flight trial are shown along with the image processing required to automate the extraction of retro-reflector returns.

1 Introduction

As part of their research into insect behaviour, entomologists often need to track their movement. It is possible to do this by visual observation for slow moving insects. However, if the insects are fast moving or if the behaviour of groups of individuals is to be monitored then visual observation becomes a problem.

The introduction of small transmitters in the last decade has made it possible to track individuals quite accurately at stand-off ranges (Hedlin and Ranius 2002; Sword, Lorch et al. 2008; Sword and Sympson 2008). However, these transmitters are expensive, and can easily be lost, making the alternative of using low-cost passive harmonic tags an advantage (Riley, Smith et al. 1996). Unfortunately, the accuracy of harmonic-radar based techniques is determined by the range and angular resolution of the radar used for this purpose, and this is generally poor. This limits the number of tagged insects that can be tracked at one time.

An alternative is to tag multiple insects with optical reflectors and track them using a camera from above, as this provides sub-pixel resolution.
As part of our collaboration with researchers from the School of Biological Sciences at the University of Sydney and the Australian Plague Locust Commission, over the last four years we have been developing what would, at first glance, appear to be an extremely simple method to track swarms of Australian plague locusts using this method. As shown in Figure 1, a collocated strobe and camera is mounted on a UAV that flies over a locust swarm.

Some of the locusts are fitted with upward pointing retro-reflective tags. The aperture and shutter speed of the camera are matched to the strobe pulse duration and intensity to minimise reflection from the ground, and only detect returns from the retro-reflectors. Repeated passes over the swarm allows the movement of the individual tagged locusts to be tracked by the positions of their retro-reflectors.

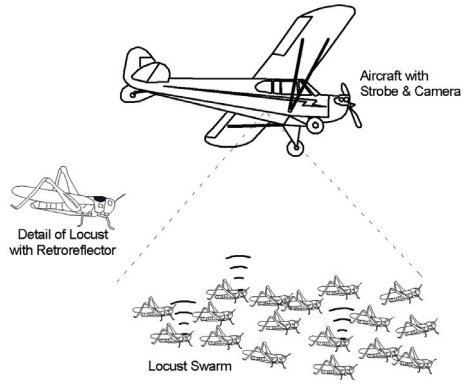

Figure 1: Principle of the strobe/camera based locust tracker

Initial results discussed in (Wendel 2008; Tahir and Brooker 2009) show that the divergence of film such as 3M Scotchlite and plastic prisms limit the power density of the reflected signal back at the camera to the extent that a maximum range of only about 50m could be achieved. This height is insufficient for the application. Subsequent tests using low divergence glass retro-reflectors proved even less satisfactory until it was realised that the reduced divergence resulted in the majority of the reflected light returning to the strobe and not the camera. This problem can be overcome by providing a common aperture for the camera and strobe.

1.1 Retro-Reflective Tag Details

To minimise the burden to the locusts and to maximise the field of view, the shortest retro-reflectors possible, are required. Unfortunately the manufacturing costs of precision ground reflectors is inversely proportional to their length so a combination of shorter and longer reflectors manufactured by Ultiquest were acquired, as shown in Figure 2. They are 2.5mm in diameter and either 4.8mm or 3.5mm long and made from BK7. The reflective surfaces are coated with Inconel (R>85%) and the entrance aperture with an anti-reflective coating (R<0.4%).

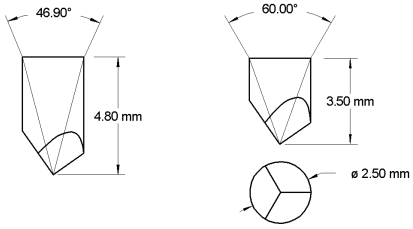

Figure 2: Diagrams of the two retro-reflector types showing the effective fields-of-view of each

Assuming that about 40% of the retro-reflective surface must be illuminated for reliable operation, then the angular fields-of-view for the two reflectors are respectively 46.9° and 60° as shown. This allows the camera to detect the reflectors over the same field-of-view, or to ensure detection if the locust-mounted reflector is at an angle, but closer to the centre of the image.

1.1 Common Aperture Options

For an operational range of 125m, the round trip time for the strobe light is only 0.8μs, therefore it is impractical (with conventional hardware) to produce sufficiently short strobe pulses with the required energy to isolate the transmitter and receiver in time. As an example, the strobe discussed in (Tahir and Brooker 2009) has a duration of more than 10μs and the camera has a similar minimum shutter time.

One alternative to achieve a common aperture is to use an optical beam-splitter. The NT54-823 cube and NT54-824 plate beam-splitters from Edmund Optics (Edmund_Optics 2011), shown in Figure 3, were tried. But even the minute amount of power reflected at the interface was sufficient to saturate the camera array.

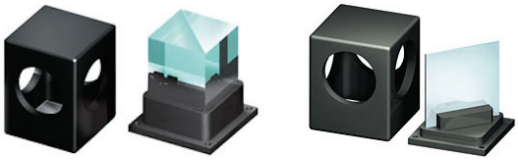

Figure 3: Edmund Optics Beam-Splitters

Another alternative is to transmit and receive through the same aperture using orthogonal polarisations. However, this requires that the tags rotate the polarisation which increases their cost.

It is also possible to maximise the effect of the small amount of divergence that occurs by capturing as much of the light as possible. Whereas, in the previous design (Tahir and Brooker 2009), the strobe and camera were arranged side-by-side, if the camera aperture surrounded that of the strobe, or visa-versa, as shown in Figure 4, then the camera would capture all of the diverging reflected light over 360°.

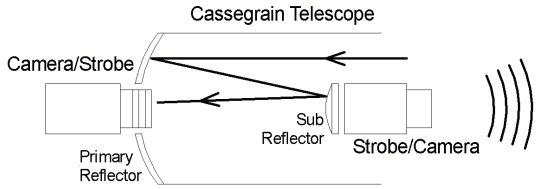

Figure 4: Camera/strobe option to maximise the amount of reflected light captured

Any divergence provided by the optical tags discussed previously is caused by a combination of surface imperfections and diffraction at the entrance/exit aperture. The divergence, θ_{div} (rad), from a circular aperture can be approximated by

$$\theta_{div} \approx \frac{\lambda}{d}, \qquad (1)$$

where λ (m) is the wavelength and d (m) is the diameter of the aperture.

For green light, $\lambda = 550\times10^{-9}$ m, and $d = 2.5\times10^{-3}$ m, the divergence will be 220 μrad. This equates to a cross-range diameter of 28mm for the retro-reflected light at a range of 125m. Therefore if the light striking the retro-reflector emanates from a point less than 28mm from the camera aperture, some of it will enter the aperture.

To test this hypothesis, measurements were conducted by Dickens using a pair of camera flash units and a circular mirror, shown in Figure 5. These were successful, with the returns from two different retro-reflectors easily detected at a range of 125m.

Figure 5: Proof of concept hardware for the collocated strobe and camera

As the camera mounting in the UAV points straight down, it is clear that the configuration shown in Figure 5 would be unsuitable. However, the same outcome would be achieved by using a ring-flash construction. Commercial ring-flash units are designed for macro work and therefore provide too little power and their light is too diffuse.

A multi-fibre light-pipe was also tried, but coupling sufficient light into and out of the pipe proved to be inefficient and poor results were obtained.

2 Strobe Implementation

In the light of the difficulties discussed, it was decided to build a completely new strobe based on an annular flash tube that could surround the camera aperture. These electronics were developed by Brooker.

2.1 Circular Flash Lamp Hardware

An appropriate flash lamp (Amglo_Kemlite 2006) with specifications as listed in Table 1, was acquired.

Table 1: Specifications of Amglo Kemlite Flash Lamp

Anode voltage (v): 500 (350-650) Flash Energy (Ws): 100 Flashes per sec: 1.1 Power: 110W Efficiency: 40 lumen/watt (typ.) Primary trigger (V): 200 Trigger transformer: VE-II Size (mm): M-10, G-7, E-24, O-31 Material: Quartz Life (flashes): 5 million	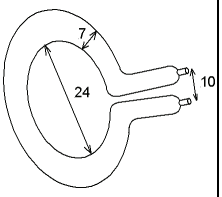

2.2 Power Supply & Triggering

A high voltage power supply, a capacitor bank and a means to trigger the flash lamp are required to make a strobe.

For UAV operation, the 500 V required, must be generated from a battery source and should therefore be as efficient as possible. A custom made power supply was provided by Lumedyne (Lumedyne 2011), along with much invaluable advice from their MD, D.J. LaDez. Unfortunately the hardware proved to be too heavy to be accommodated into the UAV, so a suitable power supply was developed using the 12QP500 DC/DC converter from Pico Electronics (Pico_Electronics 2011).

The capacitor bank should be capable of providing the rated energy to the flash lamp. Assuming that the bank discharges completely when the flash lamp is triggered, the energy available is

$$E = \frac{1}{2} CV^2, \qquad (2)$$

where E (Ws) is the total stored energy, C (F) is the capacitance of the bank and V (volts) is the capacitor voltage before discharge.

For an anode voltage of 500V, and the maximum allowed flash energy of 100 Ws, the required capacitance is 800μF. In practise, discharge is incomplete, allowing a larger capacitance to be used if required.

The Pico 12QP500 requires a battery voltage between 12 and 18V to generate a regulated output of 500V with a continuous power rating of 40W. However, this module will not start under short-circuit conditions (like charging a large capacitor), so an external bias of 17V is provided by a small DC/DC converter. The output is monitored and once the capacitor voltage reaches about 450V, the external bias is disconnected to ensure that output overload and short-circuit protection are enabled.

To minimise the possibility of conducted electromagnetic interference (EMI), all external connections (with the exception of the battery supply) to and from the trigger and HV supply are made through optical isolators.

A conventional thyristor based circuit discharges a 0.22μF capacitor through the trigger transformer to generate 11kV to trigger the flash lamp. The circuitry for this trigger is shown in Figure 6.

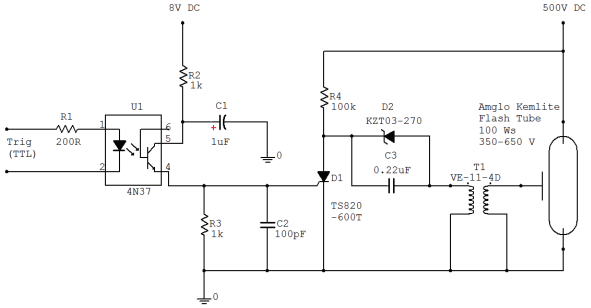

Figure 6: Strobe trigger circuit

A number of different trigger electrode configurations where tried, and while most worked after a fashion, the most consistently reliable option was a thin helix of copper wire wrapped around the flash lamp as shown in Figure 7. The two terminals of the coil are connected together to the HV terminal of the trigger transformer.

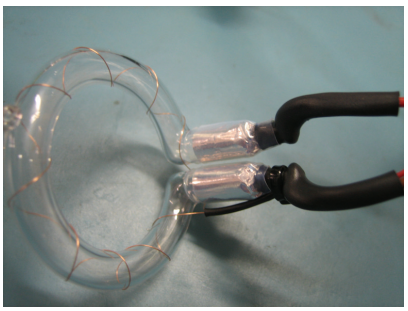

Figure 7: Trigger electrode for flash lamp

2.3 Reflector

A reflector shown in Figure 8 was manufactured using a conventional aluminium spinning process. It is designed so that the flash lamp would be at the focus of the parabolic annulus and the high sides would constrain the non-focussed portions of the beam.

Figure 8: Spun aluminium reflector prior to polishing

The interior reflecting surface was then professionally polished to an optically smooth finish.

3 Strobe Testing

To optimise the performance of the system, it is important to match the duration of the strobe with the camera shutter and to match the angular field of view provided by the camera with that illuminated by the strobe.

3.1 Strobe Duration

Using an Ames Photonics Oculus photodetector donated by Lastek (LasTek 2011), it was possible to characterise the relative power of the light generated by the strobe as a function of time. Figure 9 shows two graphs of the measured output power. The Oculus integration time is 30µs in both cases with the finer resolution graph consisting 100 delay steps each of 10µs, and the longer graph consisting of 25 delay steps each of 100µs.

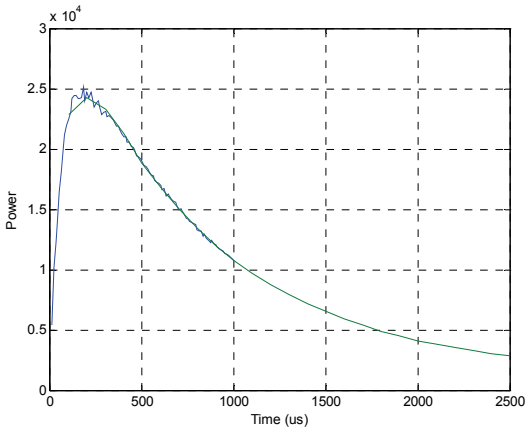

Figure 9: Occulus measurements of the optical power (arbitrary units) output by the strobe as a function of time with a 910µF capacitor bank

It can be seen that the output power reaches a maximum after only 200µs before decaying exponentially over the next 2300µs.

Integrating the optical power with time produces a measure of the energy output by the strobe, as shown in Figure 10. It can be seen that more than more than 50% of the total energy is released within the first 700µs. Therefore extending the camera shutter time beyond this would provide minimal advantage.

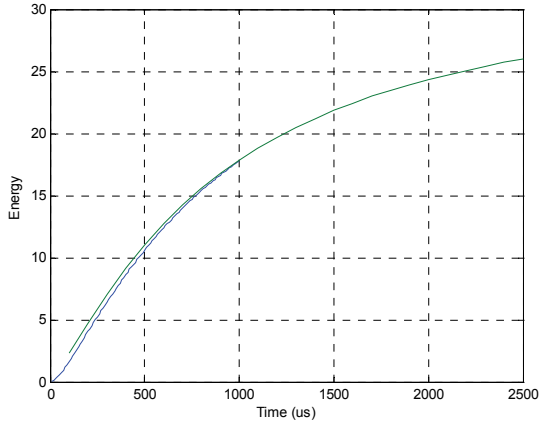

Figure 10: Calculated energy (arbitrary units) output by the strobe as a function of time

If the capacitance is reduced from 910µF to 450µF, the total energy output by the strobe is reduced proportionally, as shown in Figure 11. However what is particularly interesting is the fact that the smaller capacitance is more efficient at releasing energy initially. So, whereas it takes 700µs for the 910µF capacitor to release 50% of its energy, for the 450µF capacitor, this percentage is reached in under 400µs.

It can be concluded from these curves that the only way to shorten the discharge time significantly is to decrease the capacitance. However, if the same total energy output is required, then the charge voltage must be increased. This is limited both by the peak anode voltage of 650V for the tube, as listed in Table 1, and by the voltage rating of the capacitors (500V in this implementation).

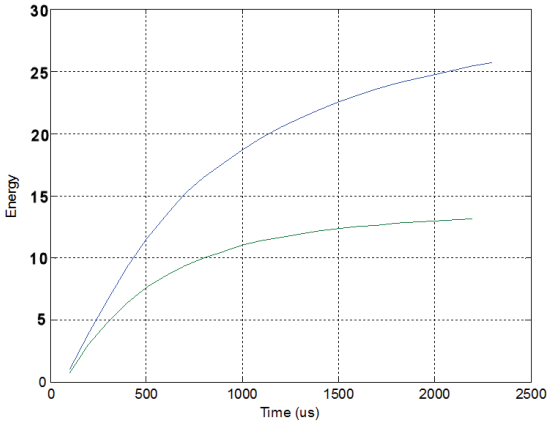

Figure 11: Comparison between the energy (arbitrary units) output by strobe as a function of time for 910µF and 450µF capacitors

3.2 Strobe Angular Field of View

Though the circular flash lamp is placed at the focus of the parabolic reflector, only those light rays radiating from the centre of the lamp along the radial plane are focussed. All of the other light rays are only constrained by the depth of the reflector. Figure 12 shows the measured angular field of view of the strobe.

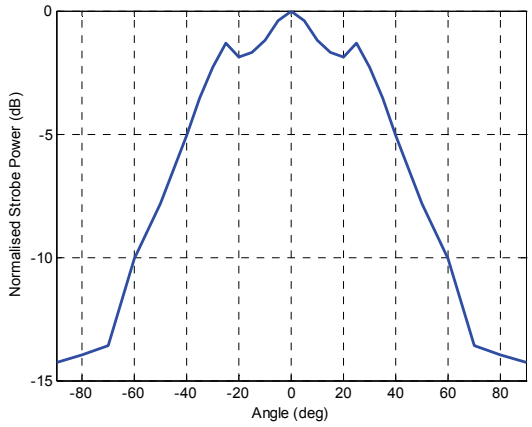

Figure 12: Measured angular field of view of the strobe

The 1/e beamwidth of the strobe is measured to be 74°, and the distance between the two outside peaks is 52° which equates quite well with the unconstrained field of view of the camera of 50.8° × 41.5°. Therefore, fairly uniform illumination of the field observed by the camera can be expected.

3.3 Complete Strobe System

The complete strobe system, shown in Figure 13, consists of the reflector enclosure which attaches to the camera bracket, and the power supply and trigger module that are housed within a shielded enclosure. A shielded cable, contiguous with the housing, extends the "faraday cage" to the strobe.

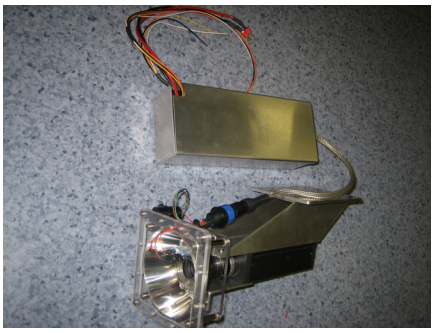

Figure 13: Photograph of the complete strobe system

3.5 Ground Test Results

Retro-reflective tags with apertures of 2.5 and 5 mm were placed on the balcony of a nearby building at a range of 125m. Tests were conducted for different aperture settings and different shutter speeds. It was found that even though the targets were visible over a wide range of settings the best contrast was achieved for an aperture setting of f4 and a shutter speed of 0.5ms, as shown in Figure 14.

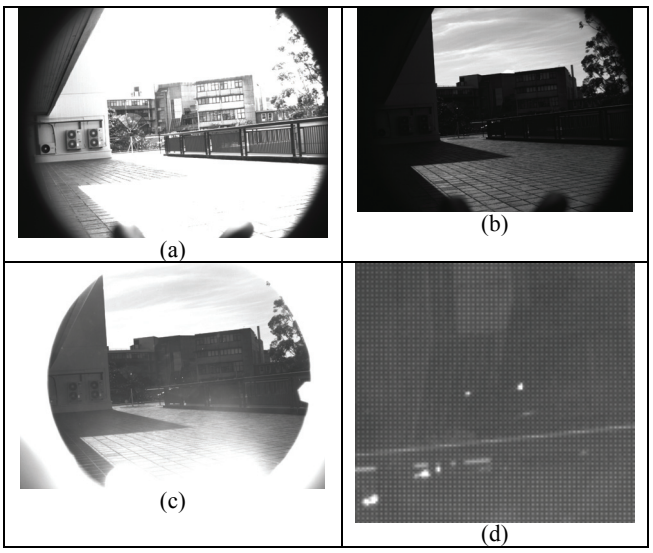

Figure 14: Images for a camera aperture of f4. a) Shutter speed optimised for ambient light b) Shutter speed set to 0.5ms c) Strobe image with shutter speed set to 0.5ms d) Expanded view showing retro reflector returns at 125m

Preliminary tests to determine the actual reflector field-of-view showed that the long 2.5mm tag was still visible when rotated away from the line-of-sight by 30º. This is better than the 23.45º half-field determined earlier.

It can be seen that the reflector produces a circular mask with a measured FOV of 42°. This is slightly smaller than the flash FOV and should therefore result in fairly uniform illumination. It is interesting to note that notwithstanding a fixed aperture, the diameter of the mask appears to be different in the ambient and the strobe images.

Some blooming can be seen at the base of the strobe image (c) which is caused by reflections from the strobe leads which are within the camera field of view.

It was also found that firing the strobe at the maximum rate (1.1 flashes per second) as specified in Table 1, generated excessive heating of the tube and reflector resulting in the breakdown of the insulating material of both the trigger and the HV supply. To cater for this during ground operation, the airflow from a small fan was directed onto the tube and reflector. However, during flight, it is assumed that natural airflow will be sufficient to cool it.

4 UAV and Payload

The UAV used for these trials is an extensively modified J3 Cub built by Randle and co-workers at the ACFR. A photograph of the aircraft along with some of the team is shown in Figure 15.

Figure 15: Some members of the locust-tracking team standing behind the J3 Cub used in the trials

The conventional RC electronics has been upgraded by the inclusion of a payload consisting of a navigation system and the strobe/camera sensor. As shown in Figure 16, the navigation system consists of an IMU, magnetometer and differential GPS interfaced to a single board PC/104 format Eden processor.

Time stamped IMU, magnetometer and differential GPS data are logged to the associated compact flash storage for later retrieval.

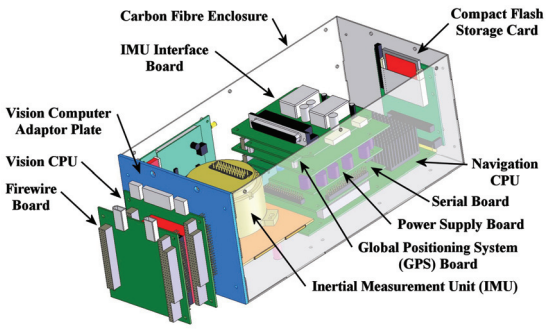

Figure 16: Graphic showing the navigation and vision payload module installed in the UAV

The strobe/camera combination is attached to the shock-mounted payload module as shown in Figure 17. To

ensure that the interior of the aircraft remains free of dust, a rubber skirt forms a flexible membrane between the body of the aircraft and the strobe reflector.

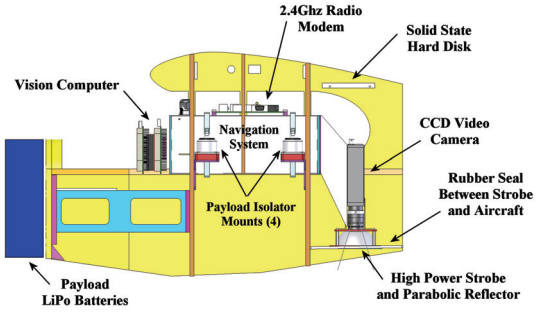

Figure 17: Installation of the Strobe/Camera system in the UAV

The camera is an IIDC 1394-based digital device - model XCD-X710CR from Sony. It is interfaced to a single board PC/104 format Intel Atom Z510/Z530 processor running the Linux Ubuntu 10.10 operating system. The software developed by Attia and Kassir which controls the camera is required to provide the following functionality:

- Synchronise the strobe and camera triggers.
- Log the images to a hard drive and metadata including camera settings and capture time.
- Adjust the exposure of the images by controlling the shutter and gain of the camera.
- Provide remote control of the application through UDP communication.

The software is written in C++ and interfaces to the Sony camera through Libdc1394, a digital camera API. All images logged to the Solid State Drive (SSD) are Bayer coded greyscale images. These can later be converted into colour images by Bayer decoding.

The software produces three types of images. Type I corresponds to a standard auto exposed image with shutter setting based on an analysis of previous frames. A type III image is obtained using a faster shutter setting and is synchronised to the strobe. Type II corresponds to an image with the same camera settings as those of type III but without the strobe. Figure 18 shows a timing diagram displaying the image capture sequence.

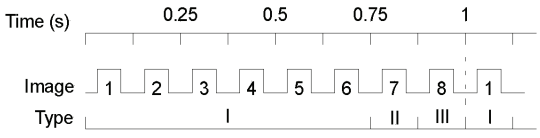

Figure 18: Image capture sequence

The correct shutter setting for images of type III minimises ambient returns while maximising reflections from the retro reflectors. The visual (type I) images are used for mapping, localisation and for visual reference. The software records the time when the image was taken and the time when it first reaches the buffer as metadata.

In order to correlate the data between the navigation data from the navigation computer and the images from the image computers, the timestamps have to be synchronised via Network time protocol (NTP). The clock onboard the Image computer is synchronised to the clock on the Navigation computer which acts as the NTP server

4.2 Integration Testing and EMI Modifications

It was found during ground tests of the complete system, that strobe generated EMI resulted in the camera PC/104 stack failing from time to time. Most of the failures were manifest as write errors to the solid-state hard drive followed by a system crash. No amount of electrical or magnetic shielding of cables, nor the application of ferrites to suppress induced voltage spikes solved the problem.

After some weeks of very frustrating experiments it was determined that the interference was probably entering the camera through its lens, and then propagating along the fire-wire cable to the PC/104 stack.

To isolate the source of interference required that the flash lamp and trigger be shielded electrically from the camera. A partial Faraday cage was built around the strobe, with the face towards the camera covered by a conductive but transparent PET sheet. Low resistivity, 10 Ohms/sq, as well as an 80% transparency is ensured by using a thin indium tin oxide (ITO) film obtained from Diamond Coatings Ltd (Diamond_Coatings 2011).

5 Flight Trials

Flight trials were conducted at the ACFR flight test centre at Marulan on 22 March 2011. A total of 14 retro-reflectors of the two kinds shown in Figure 2 were mounted on the tips of dowels and distributed around the runway. Regions containing short grass, weedy long grass and rocky terrain were selected for this deployment. To facilitate retro-reflector identification, each of these regions was marked with 400mm wooden crosses covered with retro-reflective tape. Figure 19 shows the positions of the crosses and the reflectors surveyed using RTK GPS by Chung and Xu.

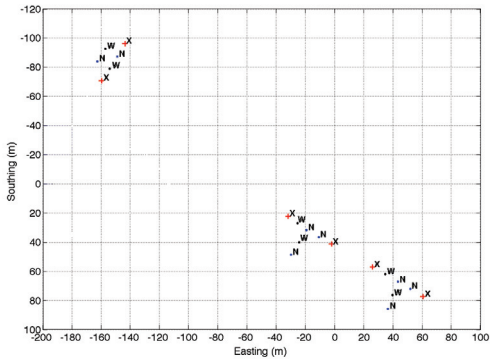

Figure 19: Navigation solution showing the surveyed positions of the crosses and the retro-reflectors

The figure labels crosses as X, the narrow field-of-view reflectors as N and the wide field-of-view reflectors as W.

5.1 Flight Path Definition

The dumbbell-shaped flight path profiles shown in Figure

20 were developed by Chung to overfly the various clusters of retro-reflectors at 70m and 100m altitudes. These are defined by series of waypoints chosen to maintain straight and level flight over the clusters to maintain good alignment of the retro-reflectors and the strobe/camera field of view.

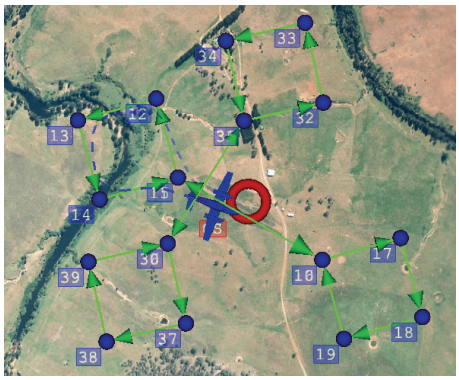

Figure 20: Aerial image of the test site at Marulan with the flight paths overlaid. The two dumbbell circuits are defined by waypoints 10 to 19 and 30 to 39.

To facilitate a smoother transition into the straight over the clusters, the turns at either end of the dumbbell were designed to accommodate the UAV's minimum turn radius followed by an additional 250m along the straight after each turn to give the UAV time to level out.

5.2 Geo-Referencing

A Kalman filter was used to fuse INS predictions with the lower update rate GPS observations. With the knowledge of the lever-arm between the INS/GPS and the camera, each of the acquired images could then be geo-referenced to the WG85 coordinate frame. Figure 21 shows part of the measured vehicle trajectory overlaid with the camera field of view and the targets on ground generated from logged navigation data by Abuhashim.

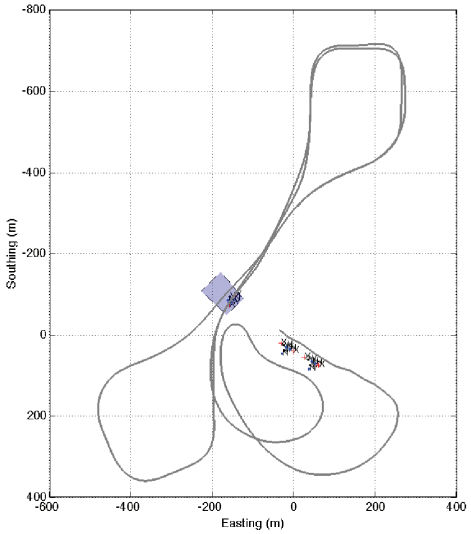

Figure 21: Snapshot of the UAV trajectory showing the unrestricted camera field of view and the predicted positions of the targets on the ground

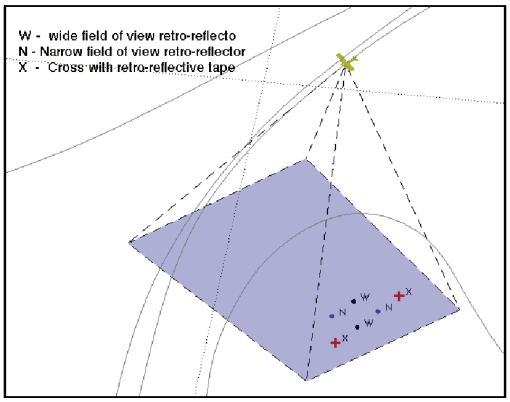

(b)

Figure 22: Magnified perspective view showing positions of the markers and retro-reflectors

5.3 Imaging Results

As discussed in Section 4, three different types of images are taken. A sample of the auto-exposed ambient image of the area, after Bayer filtering, is shown in Figure 23. Though one of the marker crosses is clear, returns from the retro-reflectors remain invisible, as expected.

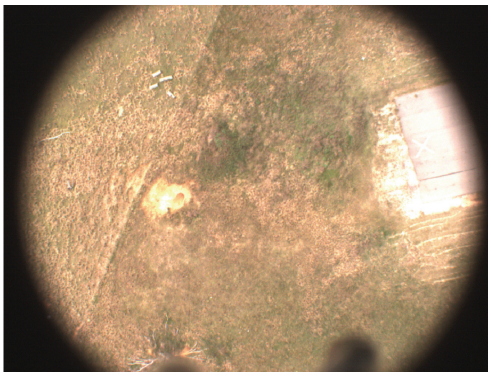

Figure 23: Visible image of the ground at the end of the runway taken at a height of 100m

5.3 Strobe-Image Processing

A Bayer filter is also used to generate a coloured image from the raw strobe-image as shown in Figure 24.

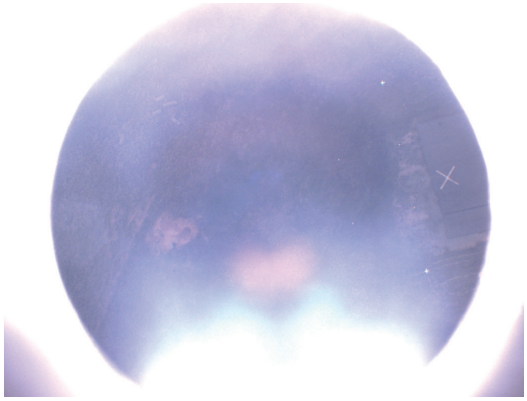

Figure 24: Strobe-image of the ground after Bayer processing

In this image, the reflective crosses are clearly visible as they subtend multiple pixels, but the retro-reflectors are still difficult to identify because they are often only a single pixel wide. The return from an individual retro-reflector can appear in any of the red, green or blue pixels, or a combination, and so can appear to be any colour.

In addition, reflected light from part of the strobe within the field of view of the camera causes considerable blooming at the bottom of the image. If this image is compared to a similar strobe-image shown in Figure 14, it is clear that the ITO film also introduces additional blooming across the whole image.

The data from a number of passes over the three clusters of retro-reflectors were examined by hand, and the individual returns identified. From a possible maximum of 106 cases where a return should have been visible, a total of 99 returns from retro-reflectors were counted. This gives a detection probability of over 93%.

The data were further processed to determine the distance of each of the reflectors from the centre of the image. As shown in Figure 25, no correlation could be found relating the relative brightness of the returns from the narrow and wide field-of-view reflectors to this distance. This might be fortuitous as, though every attempt was made to mount the reflectors pointing directly upward, there was some variation in the angle. In addition no correlation could be found between the differences in brightness of the reflectors in the centre of the image where the angle of view is 0º to those at the edges where the angle of view exceeds 20º.

Each reflector was observed between one and four times during each pass by the aircraft, and once again, there was no correlation between the amplitudes of the returns observed during this time. It is speculated that that the randomisation is a function of the interaction between the position of the point reflector and the image mosaic.

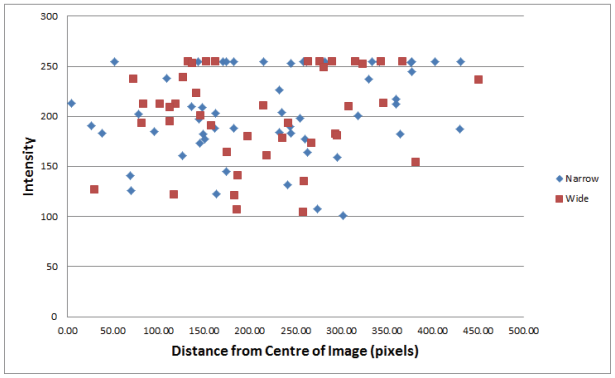

Figure 25: Measured intensity of the light reflected from the retro-reflectors as a function of their angle

It can be seen from Figure 25 that no reflectors were detected with intensities of less than 100. However, because of the nature of the raw image, as shown in Figure 26, a simple threshold cannot be applied to determine whether a reflector will be visible or not, as the apparent distributions of the red, green and blue pixels are different. Therefore a more complex process has been developed.

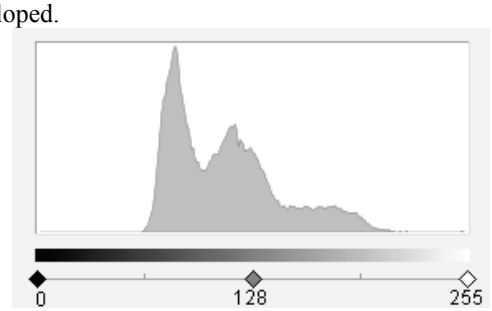

Figure 26: Histogram showing the distribution in intensity of a typical raw image, excluding the regions of blooming

This process, as illustrated in Figure 27, is required to automate the extraction the retro-reflector returns has been developed by Abuhashim. Firstly a 3×3×3 sliding window is applied to search for the maximum intensities in the three colour bands of the Bayer processed image. The central pixel in the window is assigned the maximum detected value. Following this, a low pass filter is used to generate a blurred version of the image which is subtracted from the peak-intensity image. This process removes high intensity peaks in the image due to distributed objects such as tree trunks, rocks, and foliage. Finally a circular mask is applied to remove the edges of the flash bloom before the highest peaks are extracted by thresholding.

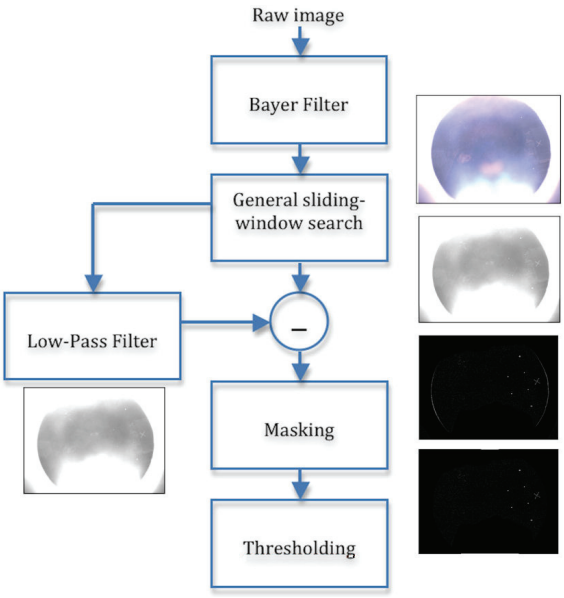

Figure 27: Processing applied to a strobe-image

All of the pixels which exceed the threshold are identified and highlighted using rectangular red boxes as shown in Figure 28. The green boxes identify the predicted positions of the retro-reflectors and the crosses as determined by their surveyed positions.

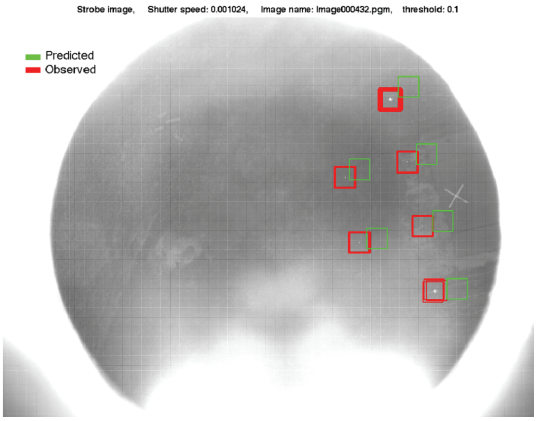

Figure 28: Rectangular markers showing the positions of the reflective crosses and the retro-reflectors superimposed onto the raw strobe-image

5.3 Locust Tagging

Retro-reflectors are sleeved with heat-shrink tubing and then glued to the upper thorax of the Australian plague locust as shown in Figure 29. The locust is also sprayed with fluorescent paint to aid with retrieval.

Figure 29: Photograph of an Australian plague locust with attached retro-reflector

Unfortunately due to inclement weather conditions, it was not possible to conduct a second flight test to determine the system performance using the tagged locusts. Notwithstanding the good results achieved with vertical mounted retro-reflectors, it is envisaged that variations in the attitudes the locust mounted reflectors, when the locusts are on the move will result in a decrease in detection probability.

6 Conclusions

A camera and strobe based system has been successfully developed with a demonstrated capability of detecting and identifying returns from 2.5mm retro-reflectors at ranges in excess of 100m. Careful consideration of the EMI generated by the strobe was required to ensure reliable operation of the UAV avionics and the sensor processor.

Though the sensor performs well, it could be improved significantly by reducing the amount of blooming. However this can only be achieved by eliminating those parts of the flash tube which are within the camera field of view.

Whether these modifications occur or not, we are confident that the system, as it stands, will be capable of tracking locusts reliably when it is deployed after the next hatchings in late spring.

References

[Amglo_Kemlite. (2006). "Circular Flashlamp." Retrieved June 2011, from http://amglo.com/circular_flashlamp.html.

Diamond_Coatings. (2011). Retrieved July, 2011, from http://www.diamondcoatings.co.uk/.

Edmund_Optics. (2011). "Online Catalog of Precision Optical Components." Retrieved July, 2011, from http://www.edmundoptics.com/products/.

Hedlin, J. and T. Ranius (2002). "Using radio telemetry to study dispersal of the beetle Osmoderma Eremita, an inhabitant of tree hollows." Computers and Electronics in Agriculture **35**: 2-3.

LasTek. (2011). Retrieved July, 2011, from http://www.lastek.com.au/.

Lumedyne. (2011). Retrieved June 2011, from http://www.lumedyne.com/.

Pico_Electronics. (2011). "QP Series." Retrieved June 2011, from http://www.picoelectronics.com/dcdclow/peQP.htm.

Riley, J., A. Smith, D. Reynolds, A. Edwards, I. Williams, N. carreck and G. Poppy (1996). "Tracking Bees with Harmonic Radar." Nature **379**: 29-30.

Sword, G., P. Lorch and D. Gwynne (2008). "A radiotelemetric analysis of the effects of prevailing wind direction on Mormon cricked migratory band movement direction." Environmental Entomology **37**: 889-896.

Sword, G. and S. Sympson (2008). "Evolution: Radiotracking Sexual Selection." Current Biology **18**: R955-956.

Tahir, N. and G. Brooker (2009). Feasibility of UAV Based Optical Tracker for Tracking Australian Plague Locust. Austlalasian Conference on Robotics and Automation (ACRA 2009). Sydney, Australia.

Wendel, A. (2008). Optical Locust Tracker. AMME/ACFR. Sydney, University of Sydney. BE Honours Thesis.